

Sensitivity studies for searches for electroweak supersymmetry during run-II of the LHC

by

Sesegma Sanzhieva

A thesis submitted in fulfilment
of the requirements for the degree of
Bachelor of Science
in Maastricht University

TABLE OF CONTENTS

ABSTRACT	iii
CHAPTERS	
I. Introduction	1
II. Background information	3
2.1 The Standard Model	3
2.1.1 The overview of the Standard Model	3
2.1.2 Limitations of the Standard Model	4
2.2 Supersymmetry	6
2.3 The ATLAS detector	7
2.3.1 The ATLAS sub-detectors and trigger systems	8
III. Search for supersymmetry at the LHC	11
3.1 Introduction	11
3.2 General search methods	15
3.3 Overview of background processes	16
3.4 Event selection and b -tagging	17
3.4.1 Event variables used in the analysis	18
3.5 Cut-and-count approach and test statistics	19
3.6 Computational tools	20
IV. Determining signal regions	21
4.1 First view	21
4.2 Applying cuts	23
4.2.1 Veto on all jets.	23
4.2.2 Veto on b -tagged jets.	24
4.2.3 Cuts in the same-flavour channel	26
4.2.4 Cuts in the different-flavour channel	27
4.2.5 Further investigation of the 200-150 signal	28
V. Conclusion	30
VI. Critical reflection	32
APPENDICES	33

ABSTRACT

CHAPTER I

Introduction

High Energy Physics (HEP) is a branch of physics that studies elementary particles. The main way of studying physics experimentally at subatomic level is analysing information from particle collisions. Specific particles are accelerated to high speeds and directed to collide with each other producing an array of other particles that are then registered by detectors and studied by physicists. The largest currently functioning HEP experiment is the Large Hadron Collider (LHC) at CERN in Geneva, Switzerland. Since 2015, it is able to accelerate protons and create collisions at a centre-of-mass energy of 13 TeV. These collisions happen at two sites where the main particle detectors are situated. These experiments are ATLAS (A Toroidal LHC Apparatus) and CMS (Compact Muon Solenoid). Such high energy conditions of collisions emulate the state of the universe very shortly after the Big Bang and thus allow creation of particles that do not exist at normal conditions.

The underlying theory of modern HEP is the Standard Model (SM) and it has been very successful in describing subatomic particles and the interactions between them. It is a very robust theory that has been tested through a plethora of experiments at colliders. The most prominent success of previous LHC runs at 7 and 8 TeV centre-of-mass energy was the discovery of the Higgs particle, which was the final SM particle whose existence was proven experimentally [1, 2].

However, there are limitations to SM and there are a number of theories that try address these shortcomings. Collectively they are known as Beyond-the-Standard-Model (BSM) theories and present new theoretical frameworks aiming to explain physical world at a deeper level. One of the major BSM theories is supersymmetry (SUSY). It has a mathematically effective and elegant representation and, most importantly, overcomes some critical SM limitations.

Searches for evidence of supersymmetry are performed at the LHC along with other particle experiments. After runs at 7 and 8 TeV no significant evidence was

found and limits on masses of hypothetical supersymmetric particles have been placed. Higher energy collisions present a better chance of finding evidence of supersymmetry. The research presented in this thesis focuses on trying to design search methods in run-II (13 TeV) data that are sensitive to particular SUSY scenarios that feature electroweak production and decay. For that purpose a set of kinematic and topological variables are investigated as ways to determine presence of new particles.

CHAPTER II

Background information

2.1 The Standard Model

2.1.1 The overview of the Standard Model

The underlying theory of modern High Energy Physics is the Standard Model (SM). This theory has been developed in the second half of the 20th century with contributions from many scientists and it is a very successful representation of the world on the subatomic level. The SM classifies all known subatomic particles into specific categories and provides the description of the interactions between them.

In the SM there are two main types of fermions (1/2-spin particles) known as quarks and leptons. Each family has three generations with each consecutive generation being heavier than the previous. The up and down quarks along with the electron are stable and constitute ordinary matter. The interactions between fermions are mediated through the exchange of force carrier particles known as gauge bosons (see Tab. 2.1). The final piece in the SM is the Higgs boson and it gives mass to other fundamental particles. All bosons possess integer spin [3]. Further nomenclature identifies hadrons - composite particles that are made of quarks and gluons.

The mathematical representation of the SM is built within the broader frame of Group Theory. Employing the official terminology, the SM has the symmetry group

Fermion	Generations			Bosons
Leptons	e	μ	τ	Z
	ν_e	ν_μ	ν_τ	W^\pm
Quarks	u	c	t	photon
	d	s	b	gluon

Table 2.1: The Standard Model particles

$U(1)_Y \times SU(2)_L \times SU(3)$. The $SU(3)$ symmetry group generates strong interactions, that describe processes involving quarks and gluons. These processes are described by the theory of Quantum Chromodynamics and the particles possess a specific type of charge known as “colour charge”. The $U(1)_Y \times SU(2)_L$ group generates electroweak interactions. At energies below 100 GeV, however, the single electroweak interaction is broken into the weak and electromagnetic varieties with the symmetry group $U(1)_{em}$. The unification of these two types was the result of efforts by Glashow, Weinberg and Salam [4, 5, 6]. The weak interaction processes involve fermions and are mediated by electrically charged W^\pm bosons for charged processes and the chargeless Z gauge boson for neutral ones. Finally, the electromagnetic force is mediated by photons and only involves electrically charged particles.

Above the unification energy of 100 GeV, and thus before the spontaneous electroweak symmetry breaking through Higgs mechanism [7, 8], the gauge bosons are different. There are three W bosons, denoted W^1 , W^2 , W^3 corresponding to the $SU(2)_L$ part of the group and one B boson corresponding to the $U(1)_Y$ part. All the electroweak bosons are massless, and acquire mass by coupling to the Higgs field in the process of symmetry breaking.

2.1.2 Limitations of the Standard Model

The predictions of the SM have been successfully tested in particle accelerator experiments, and its final confirmation came with the discovery of the Higgs boson in 2012 - a true scientific breakthrough. This was the last missing piece of experimental evidence needed for the full validation of the SM. The experiments that led to this discovery were conducted at CERNs Large Hadron Collider (LHC) in run-I proton-proton collisions at centre-of-mass energy $\sqrt{s} = 7$ and the later upgrade to 8 TeV. Despite the fact that the SM has proven to be an extremely precise and successful theory there are some caveats for which it does not provide adequate solutions.

One of the inconsistencies within the SM is the so-called Hierarchy problem [9]. One of the ways it reveals itself is through the large discrepancy between the Planck mass and the mass of the Higgs particle. The former is about 10^{17} times bigger than the latter and current representation of particle physics cannot explain such a big difference. Quantum effects start manifesting themselves at the Plank mass threshold and such a vast difference between these two values is yet unaccounted for.

Another prominent problem is that the SM does not explain dark matter. While ordinary matter only constitutes about 5% in the total mass-energy content of the universe, it is dark matter and dark energy that account for the rest [10]. The SM

does not provide a candidate particle for dark matter and thus is only able to describe ordinary matter and energy.

One of the main challenges of modern physics is the unification of forces. This is part of the ongoing attempts to reach the ultimate goal - a “theory of everything”. Such a theory would have to account for all physical aspects of the universe and include the most fundamental structures and interactions. The first step was made with the unification of electromagnetic and weak forces. The next step is to achieve the unification of electromagnetic, weak, and strong interaction forces this step is the Grand Unification. The ultimate step is to combine all four fundamental forces together, which means adding gravity, in what is called Super Unification (see Fig. 2.1). Thus far quantum field theory and general relativity are able to describe phenomena on their respective scale of action with remarkable precision, but are fundamentally incompatible.

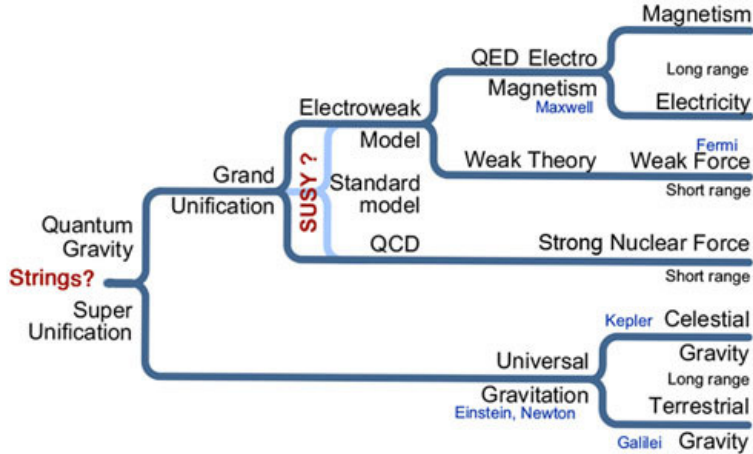


Figure 2.1: Various stages in the unification of forces [11]

Within the confines of the SM even the Grand Unification is not possible, and this prompts the search for new theories that account for this and other shortcomings of the SM. Collectively they are called Beyond-Standard-Model (BSM) theories. Among these, there are theories that include extra-dimensions, composite Higgs boson models, etc. Theoretical and experimental search for BSM physics is the current frontier of HEP and one of the most important questions in science overall.

2.2 Supersymmetry

One of the strongest candidate framework theories that can offer solutions to the SM deficiencies is supersymmetry (SUSY) [12]. SUSY is a spacetime symmetry that equates fermionic and bosonic degrees of freedom. Among several theories that are based on SUSY principles, the Minimal Supersymmetric Standard Model (MSSM) offers the simplest extention of the SM. The MSSM postulates that each SM particle has a supersymmetric partner which is different only in spin by one-half unit while all other quantum numbers stay the same. The superpartners of quarks, leptons, and neutrinos are called squarks, sleptons and sneutrinos. For gauge bosons the superpartners are gluinos, photino, winos and binos, collectively named gauginos. The latter two are superpartners of the B and three W bosons of the elecrownreak interaction before electroweak symmetry breaking. It follows naturally since SUSY is invoked before the electroweak symmetry breaking. The Higgs sector in SUSY has five superpartners - two charged (H^\pm) particles and three neutral ones (h^0, H^0, A^0). They are known collectively as Higgsinos. Mixing between winos, binos and Higgsinos results in charginos and neutralinos. Their mass eigenstates are referred to as $\tilde{\chi}_i^\pm$ ($i = 1,2$) and $\tilde{\chi}_i^0$ ($i = 1,2,3,4$) in order fo increasing mass.

The MSSM belongs to a class of theories that all share the same requirement - a quantity known as R-parity has to be conserved in interactions. The mathematical description of R-parity is beyond the scope of this paper. However, one important consequence of R-parity conservation is that if supersymmetric particles were to be produced in collisions, they would be created in pairs. Then they decay through various possible scenarios with the lightest supersymmetric particle (LSP) emerging in the final state and escaping undetected. Because the LSP is stable it provides a possible candidate for the dark matter particle.

The MSSM imposes 105 free parameters and this is one of its major issues, since any analysis will be addled with enormous complexity stemming from high dimensionality. There are various simplified models that reduce the number of free parameters to manageable values through various theoretically and experimentally motivated constraints. One of them is the phenomenological Minimal Supersymmetric Standard Model (pMSSM) that contains only 19 free parameters and which will be used in this thesis' analysis.

2.3 The ATLAS detector

The ATLAS experiment is a multi-purpose particle detector with cylindrical geometry and has a nominal forward-backward symmetry [13]. The dimensions of the detector are 25 m in height and 44 m in length and the overall weight of the detector is approximately 7000 tonnes. It can detect particles with almost 4π coverage in solid angle around the collision point, which covers almost all of the spherical area around the center.

Proton bunches are accelerated in the underground ring that is 27 km in diameter and are directed to collide inside the detectors. The collisions happen at 40 MHz bunch crossing rate, with an average 23 interactions per bunch crossing. The LHC is designed to operate at $\sqrt{s}=14$ TeV and instantaneous luminosity $\mathcal{L} = 10^{34}$ cm $^{-2}$ s $^{-1}$ in proton-proton collision mode. Instantaneous luminosity is defined as follows

$$\mathcal{L} = \frac{1}{\sigma} \frac{dN}{dt} \quad (2.1)$$

Where σ is the interaction cross-section, and N is the number of detected events during time t . Integrated luminosity $\int \mathcal{L} dt$ is a quantity that expresses the amount of total data gathered during the time t of running the LHC. Luminosity is particularly useful as a way to express the amount of data gathered, because it allows to find number of events for a particular process simply by multiplying this process's cross-section by the value of luminosity. The analysis presented in this paper uses the dataset recorded at 3.2 fb $^{-1}$ of integrated luminosity throughout run-II of the LHC during 2015.

The Cartesian coordinate system used at ATLAS has its origin at the nominal point of interaction with the z axis extending along the particle beam longitudinally, the positive x axis pointing towards the center of the ring, and the positive y axis pointing upwards. The geometry of the detector makes the use of cylindrical coordinate system especially convenient. Using it, the z axis stays the same, the polar angle θ is the angle from the z -axis, and the azimuthal angle ϕ encircles the z axis in the transverse plane. However, instead of θ it is more convenient to use pseudorapidity η , due to the fact that differences in pseudorapidity are close to invariant under Lorentz boosts along the z axis (fully invariant for real rapidity). η is defined as follows

$$\eta = -\ln\left(\tan \frac{\theta}{2}\right) \quad (2.2)$$

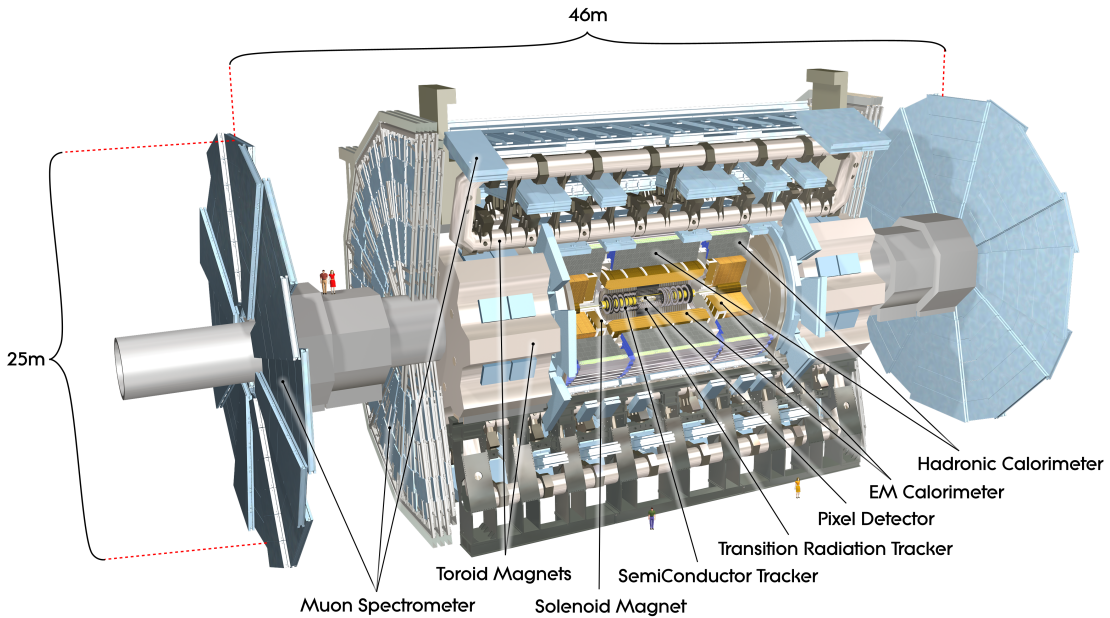


Figure 2.2: Cut-away view of the ATLAS detector (people are included for scale comparison) [13].

2.3.1 The ATLAS sub-detectors and trigger systems

The ATLAS detector consists of several subdetector layers with each layer performing a specific function (see Fig. 2.3). The Inner Detector (ID) performs tracking of newly created particles. It is closest to the collision point and covers $|\eta| < 2.5$ in pseudorapidity. The ID has high granularity as it is exposed to the highest density of particle interaction. It was designed to provide a transverse momentum resolution and a transverse impact parameter resolution [14]. The detector itself consists of three separate subsystems. The main components of the ID are the silicon pixel detector, the semiconductor tracker, and the transition radiation tracker. Ahead of the run-II a new pixel layer, called the Insertable B-Layer (IBL), has been added to the ID improving the resolution and particle identification qualities. All these layers are immersed in a 2 T magnetic field, created by the thin superconducting solenoidal magnet. This field is parallel to the beam axis and bends trajectories of charged particles allowing their charge and momentum identification based on the characteristic bending of their trajectories.

The next two layers are the two calorimeters that measure energies of specific types of particles. The particles travel through the detectors and lose their energy via

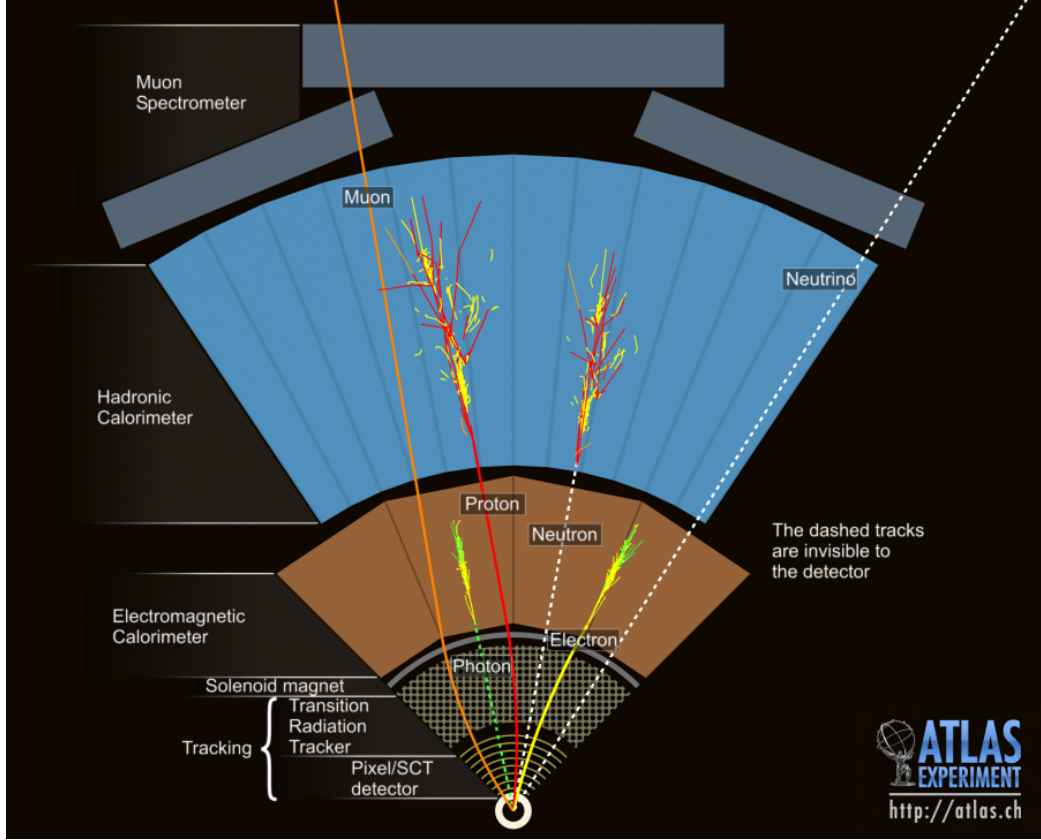


Figure 2.3: Event in the transverse plane, a computer generated image of the ATLAS detector [15].

interaction with its layers leaving energy deposits as they move through the material. The first one is the high-granularity Electromagnetic Calorimeter (EmCal) and it measures energies of electrons and photons. Coloured particles (gluons and quarks) form “jets” that travel further into Hadronic calorimeter (HCal) where they continue their decays and also deposit their available energy. Both calorimeters are designed to provide good quality measurements of momentum and energy and cover the region $|\eta| < 4.9$.

The final detecting layer is the Muon spectrometer (MS), which tracks and measures charged particles, specifically muons. Muons do not interact with matter as strongly as electrons so they travel further without radiating much energy in the calorimeters. The MS is immersed into a large toroidal magnet, that provides a magnetic field throughout the spectrometer and bends the trajectories of charged muons, which makes it possible to detect their charge and momentum. Any particles that are not covered by the described sub-detectors will escape undetected. These include neutrinos and, possibly, the LSP.

Triggers are used to select events by identifying signatures of various particles as well as using global event signatures, such as missing transverse energy [16]. A multilevel trigger system is used at ATLAS to select events that are of interest to further offline analysis. The first level is hardware-based and uses information from the calorimeters and muon spectrometer, the second and third levels are software-based and use information from all sub-detectors. Because the data at the LHC is produced in staggering amounts employing efficient trigger systems is crucial to be able to extract information that is relevant for further analysis. At $\sqrt{s}=13$ TeV the spacing between bunches crossing is 25 ns and the collision rate is 40 MHz. This rate has to be reduced to $O(500$ Hz) to be able to keep data in permanent memory devices [17].

Ideally, a trigger should be able to retain a maximum number of events that are interesting for physics analysis and reject as many background events as possible. In this regard the concept of trigger efficiency is very important, and this efficiency varies depending on the particular process that is being investigated. The overall goal is to reduce data from the raw amount to the size at which it can be stored permanently and at the same time keeping as many relevant events as possible.

CHAPTER III

Search for supersymmetry at the LHC

3.1 Introduction

Searches for various BSM theories including SUSY have been performed at the LHC alongside searching for the Higgs and performing different SM analyses. Many SUSY searches were conducted targeting the production of squarks and gluinos. This was motivated by a larger theoretical cross-section and therefore higher probability of producing coloured superpartners [18]. Up to this moment no statistically significant excess over the SM has been detected and exclusion limits were placed on masses of SUSY particles. Figure 3.1 shows the latest data on the masses that have been excluded for supersymmetric particles in various production scenarios. The lower limits on the masses of most squarks and gluinos in different searches significantly exceed 1 TeV [19]. As a consequence, if their production occurs, it is either extremely rare at present energies or requires higher energy of collision to leave an identifiable signature.

This thesis's research will focus on the electroweak production as one of the possible SUSY particle production scenarios. Sleptons and gauginos are produced in electroweak production processes and are not affected by the strong force. They have smaller cross-sections compared to squarks and gluinos, so their theoretical production rate is smaller. However, if their masses are small compared to the strongly interacting sparticles, SUSY production will likely be dominated by electroweak production where sparticles have smaller mass. Current centre-of-mass energy might be enough to produce them in quantities that would allow their detection [20].

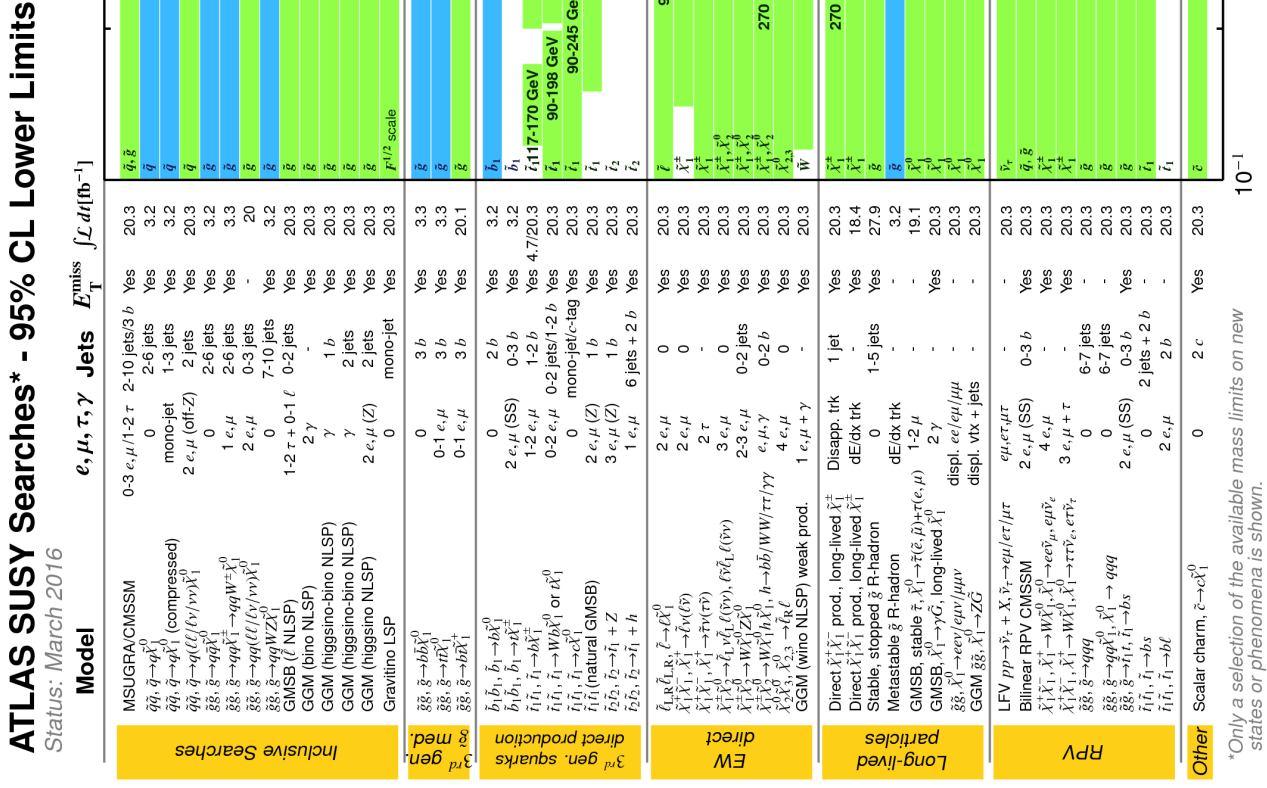


Figure 3.1: Exclusion limits of ATLAS searches for Supersymmetry. Squark and gluon masses are predominantly above the 1 TeV. [21]

So far searches in the electroweak region have been unable to find evidence of supersymmetric particles. Limits on their masses according to various decay scenarios have been obtained and can be seen in Fig 3.2.

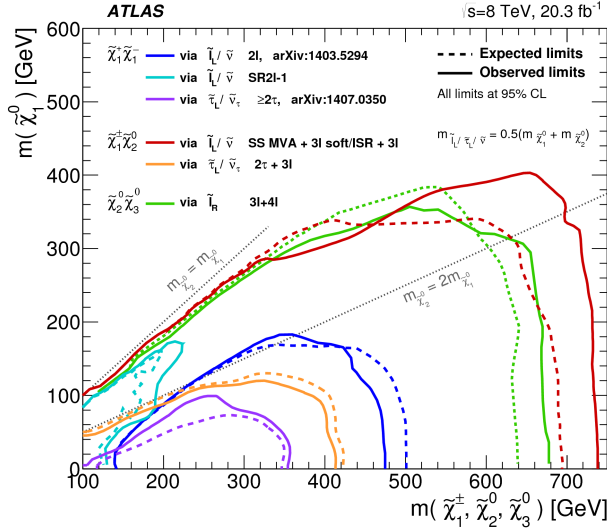


Figure 3.2: The 95% CL exclusion limits on $\chi_1^+ \chi_1^-$, $\chi_1^\pm \chi_2^0$ and $\chi_2^0 \chi_3^0$ production with $\tilde{\ell}$ -mediated decays, as a function of the χ_1^\pm , χ_2^0 and χ_3^0 masses [22].

These results are taken from the analysis performed at $\sqrt{s} = 8$ TeV and integrated luminosity of 20.3 fb^{-1} [20]. The search was performed based on various scenarios of the MSSM, involving electroweak production of charginos and neutralinos. The turquoise and blue lines represent decay scenarios that are relevant for this paper as they show information on slepton-mediated decays of a chargino pair. In particular, the production of a $\tilde{\chi}_1^+ \tilde{\chi}_1^-$ pair decaying through a slepton ($\tilde{\ell}$) with final states containing two opposite sign leptons will be considered (see Fig. 3.3).

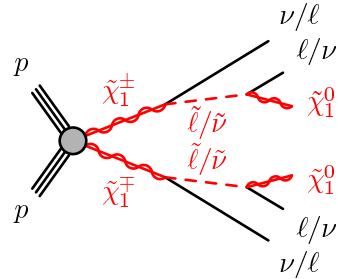


Figure 3.3: Electroweak chargino pair production in proton-proton collisions with intermediate slepton in the decay process.

In this thesis three different patterns of mass-splitting between the chargino and the neutralino will be considered. Denoted by the pair of numbers assigned to the masses in GeV of the chargino and the neutralino respectively, they are 600-100, 400-200, and 200-150 signal models. The choice for these signals is motivated by the fact that they are not covered by the exclusion limits shown in Fig. 3.3 and their variety in terms of mass splitting. For all of them the mass of the intermediate slepton is set to be $m_{\tilde{\ell}} = 0.5(m_{\tilde{\chi}_1^\pm} + m_{\tilde{\chi}_1^0})$.

The cross-section of the investigated production process depends on the mass of the chargino - lighter ones are more likely to be produced and therefore have a larger cross-sections. Fig. 3.4 shows the distribution of the theoretical cross sections depending on the mass of the chargino. For the models used in this thesis the cross sections are $902.569(\pm 53.741)$ fb $^{-1}$ for the 200 GeV chargino, $58.631 (\pm 4.728)$ fb $^{-1}$ for the 400 GeV, and $9.499(\pm 0.912)$ fb $^{-1}$ for the 600 GeV one. The cross sections for this process were obtained from [23, 24].

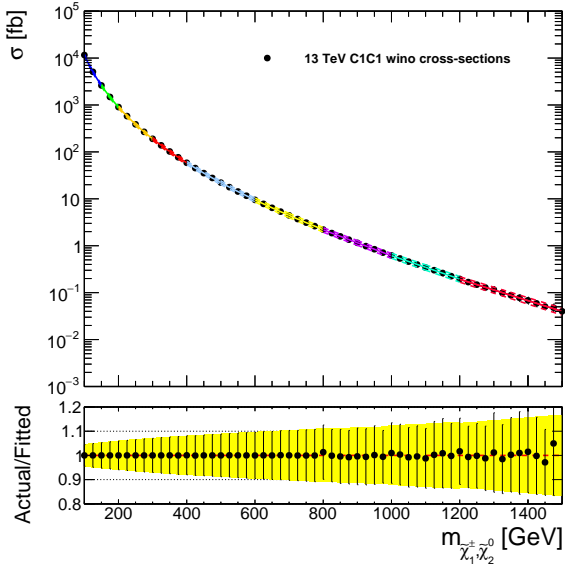


Figure 3.4: The distribution of cross-sections for slepton-mediated chargino decay [25].

In the nomenclature used at LHC and in this thesis, electrons and muons are called “light leptons”. Taus are considered separately as they decay very promptly and therefore are very difficult to reconstruct. This thesis only focuses on final states containing electrons and muons and thus the designation “lepton” only refers to these particles.

3.2 General search methods

Detecting new physics events at LHC requires using computational and statistical methods that can deal with the type of information a particle accelerator produces. The data is initially collected using triggers corresponding to the type of events under analysis. Each event has a large number of physical characteristics such as momentum, energy, mass, multiplicities, etc. The numbers representing them are all stored in a data structure which then can be accessed, modified and analysed using software tools.

The cornerstone of all accelerator physics analyses is the correct estimation of background events. All background events represent physics that is already known and that has some similar or identical features with the processes under investigation. For instance, this thesis focusses on the reactions that have precisely two oppositely charged leptons in their final states. A number of processes well described by the standard model share this characteristic and therefore will form the background.

The task of correctly identifying background is therefore crucial in the process of searches for new physics events. Monte Carlo (MC) simulations are used to generate background events distribution samples according to a probability density function of a particular process. In this thesis MC simulated data samples are used to model SM background events along with SUSY signal events. All the samples include events that can result in dileptonic decays.

The data is then overlaid on the simulated background to see whether there is a disagreement between data and background. If there is a significantly large excess of data over background it can lead to new discoveries such as the existence of a new particle. The presence of a new particle can reveal itself in a number of ways. The straightforward way to detect a new physics event is an abnormality in some distribution of the data, as was the case with the discovery of the Higgs (see Fig. 3.5). The narrow peak over a smooth line in mass distribution of diphoton events constituted a significant excess over the SM predictions and was in agreement with theoretical predictions [1].

Unfortunately, this method does not work well for SUSY particles and other techniques have to be used. Standard search techniques involve defining **signal regions** in data distributions that are sensitive to possible SUSY signals and looking whether there is a significant excess over the SM background predictions in these regions. This also includes looking for abnormal tails in distributions of different variables that are not in agreement with the SM predictions. These variables will be discussed in the

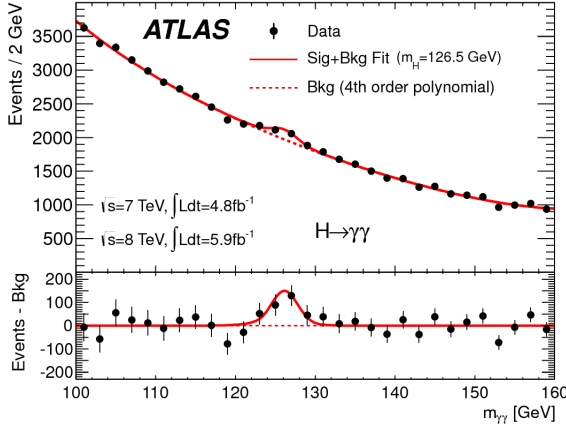


Figure 3.5: Invariant mass distribution of diphoton candidates for the combined $\sqrt{s} = 7$ TeV and $\sqrt{s} = 8$ TeV data samples. The mass of the Higgs corresponds to the peak at 126.5 GeV [1].

subsection 3.4.1. Signal regions are usually determined using the “cut-and-count” approach that will be discussed in the section 3.5.

3.3 Overview of background processes

In order to distinguish new physics events from the SM events it is necessary to be able to suppress all SM events that have the same final state. Within the scope of this thesis that includes events that have precisely two leptons with opposite charge. The processes described in this section constitute MC simulated background that was used in the search for signal regions.

The Z +jets background comes from the production of jets of particles in association with a Z boson or a virtual photon (Drell-Yan process), which then decays into two leptons. $t\bar{t}$ pair creation is a common process in pp collisions and is one of the dominant processes in dilepton decays. The quark-antiquark pair decays via the $W^+bW^- \bar{b}$ intermediate state into three different final states with either no leptons, one lepton, or two leptons (here leptons include the tau). The latter decay cascade is $t\bar{t} \rightarrow W^+bW^- \bar{b} \rightarrow \ell\nu\ell\nu b\bar{b}$. Final states that include electrons and muons constitute around 5% of the entire $t\bar{t}$ production [26]. Thus, the $t\bar{t}$ production is one of the main background processes in searches for BSM events in various channels, not only those involving two-lepton final states.

The diboson production channel is dominated by the production of the WW pair with subsequent decay into two lepton/neutrino pairs. Contributions also come from the ZV channel, where $V = W$ or Z . Other sources of dilepton final states are W +jets

and single-top quark production processes. Both of them have a decay channel with final states containing a lepton and a neutrino, however their overall contribution to the background is small compared to diboson, $t\bar{t}$, and $Z+\text{jets}$. All the MC background predictions used in this thesis belong to one of the categories described in this section.

A serious hindrance in LHC analyses is the phenomenon of “pileup”. Among the collisions that produce events of interest there are additional collisions that contaminate the output with extra jets. Along with this, tighter spacing between bunches means that for a specific collision, additional jets might originate from a neighbouring collision as the sensitivity windows for many ATLAS subsystems are longer than 25 ns [27]. Dealing with the increased pileup presents an additional challenge at the $\sqrt{s} = 13$ TeV run, because of additional jet contamination of the data.

3.4 Event selection and b -tagging

Event reconstruction is the process of turning raw data into manageable format that includes quantities needed in physics analysis. An event has to pass certain identification criteria to be chosen for reconstruction. Correct identification of different physics objects at LHC includes a large number of dedicated algorithms which are not presented in this thesis, but are available elsewhere [28]. However, in this section a very general outline of the selection procedure for reactions that result in two leptonic decays will be given. All “signal” objects must have passed a set of criteria to obtain a high quality sample with minimum possible contamination.

Signal electrons are required to have $|\eta| < 2.47$ and transverse momentum $p_T > 10$ GeV. These are inferred from the calibrated energy deposits in the EmCal and must have a matching ID track. Signal muons are reconstructed using information from MS and ID tracks and are required to have $|\eta| < 2.5$ and $p_T > 10$ GeV. Jets are reconstructed using information from calorimeters and are divided into “central” and “forward” categories. Central jets must have $|\eta| < 2.4$ and $p_T > 20$ GeV. Forward jets are those with $2.4 < |\eta| < 4.5$ and $p_T > 30$ GeV.

One of the common techniques used in LHC analyses is the identification of central jets that have b -hadrons (hadrons containing bottom quark/s). These jets are referred to as b -tagged and are identified using multivariate techniques based on machine learning instruments such as artificial neural networks and boosted decision trees [29]. The efficiency of b -tagging has been significantly improved in run-II due to the addition of the Insertable B-Layer in the ID. b -tagging is an extremely useful technique because some important heavy particles such as top quark and the Higgs

decay into bottom quarks.

3.4.1 Event variables used in the analysis

A set of discriminating variables associated with searches for evidence of SUSY is presented here. Topological and kinematic variables as well as quantities derived from them will be investigated.

\mathbf{p}_T^X The transverse momentum of an object X .

$\Delta\phi(\mathbf{X}, \mathbf{Y})$ The difference in the azimuthal angle between two reconstructed objects X and Y , e.g. $\Delta\phi(E_T^{miss}, \ell)$.

E_T^{miss} The magnitude of the missing transverse momentum of the event. Missing transverse momentum is defined as the negative vector sum of the transverse momenta of all identified objects.

$E_T^{miss,rel}$ This value is defined as

$$E_T^{miss,rel} = \begin{cases} E_T^{miss} & \text{if } \Delta\phi(E_T^{miss}, \ell/j) \geq \pi/2, \\ E_T^{miss} \times \sin\Delta\phi(E_T^{miss}, \ell/j) & \text{if } \Delta\phi(E_T^{miss}, \ell/j) < \pi/2 \end{cases}$$

where $\Delta\phi(E_T^{miss}, \ell/j)$ is the azimuthal angle between the direction of $E_T^{miss,rel}$ and that of the nearest electron, muon, or central jet.

$m_{\ell\ell}$ The invariant mass of the two leptons.

Another derived event variable is the so-called “stransverse mass” m_{T2} which was introduced as a way to infer information about undetected particles [30, 31]. Along with that, it is also proved useful in suppressing backgrounds. It is used to bound the masses of a pair of supersymmetric particles, each of them decaying into one visible and one invisible particle. It is a function of the momenta of two visible particles and the missing transverse momentum of an event. Its abbreviated mathematical description is as follows

$$m_{T2} = \min_{\mathbf{q}_T} \left[\max \left(m_T(\mathbf{p}_T^{\ell 1}, \mathbf{q}_T), m_T(\mathbf{p}_T^{\ell 2}, \mathbf{p}_T^{miss} - \mathbf{q}_T) \right) \right], \quad (3.1)$$

where $\mathbf{p}_T^{\ell 1}$ and $\mathbf{p}_T^{\ell 2}$ are the transverse momenta of the two leptons, and \mathbf{q}_T is a transverse vector that minimizes the larger of two transverse masses m_T which is defined

as

$$m_T(\mathbf{p}_T, \mathbf{q}_T) = \sqrt{2(p_T q_T - \mathbf{p}_T \cdot \mathbf{q}_T)}. \quad (3.2)$$

The m_{T2} has an upper end at the W mass for SM $t\bar{t}$ and WW events, where the missing momentum originates from neutrinos. In cases with signal events, where the LSP contributes to $\mathbf{p}_T^{\text{miss}}$, the m_{T2} endpoint is correlated to the mass difference between the chargino and the lightest neutralino. m_{T2} is more sensitive to large mass splittings as its distribution then extends significantly beyond the distributions of $t\bar{t}$ and WW events. Its performance decreases for signals with small mass splittings.

3.5 Cut-and-count approach and test statistics

As discussed previously, a good signal region retains as many signal events as possible while at the same time cutting out background events. The way to suppress the background is to use successive cuts. The cuts are based on determining physical quantities that are able to discriminate between signal and background. The choice for a single cut is motivated both by theoretical considerations and the shapes of the MC signal and background distributions.

To optimize a cut or a set of cuts a metric that shows their discriminating power is needed. The numerical expression of how well a cut performs is given by a score function and its result will be referred to as “significance”. The score function is constructed in the following way. The total number of events in a particular selection is N , and it is the sum of S and B . The latter two refer to the number of signal and background events respectively. This gives the following expression

$$S = N - B \quad (3.3)$$

The uncertainty of S is then

$$\sigma^2(S) = \sigma^2(N) + \sigma^2(B) = N + \sigma^2(B). \quad (3.4)$$

N is a mean value of a distribution described by Poisson statistics where the uncertainty is $\sigma = \sqrt{\lambda}$, so squaring it back just yields N . $\sigma(B)$ is the uncertainty on the estimated average of the B value. Because estimation of the background is done with large MC statistics the $\sigma(B)$ in this case can be treated as negligible. So what is left is

$$\frac{S}{\sigma(S)} = \frac{S}{\sqrt{N}} = \frac{S}{\sqrt{S+B}}. \quad (3.5)$$

This determines the number of standard deviations away from the 0 of the signal. Due to SUSY signals being very small compared to the background, further simplification can be done, so that the above expression becomes

$$\frac{S}{\sigma(S)} \simeq \frac{S}{\sqrt{B}}. \quad (3.6)$$

The process of scientific discovery relies predominantly on using statistical methods to justify new discoveries and safeguard against false ones. It is especially important in HEP as it operates on quantum level where almost everything is described using probabilistic arguments (a particle’s wave function being the most obvious example).

Any potential discovery in HEP must comply with stringent requirements posed by statistical inference. If some signal has a mean that is away from the mean of the background-only sample by three standard deviations (3σ), it is referred to as “evidence”. If it is a 5σ event then it is claimed as a discovery. To put this into perspective, the chance of a 5σ event being just random fluctuation is around 1 in 3.5 million. The expression S/\sqrt{B} thus is a rough estimate of the number of standard deviations and can serve as a metric to assess the quality of candidate signal regions.

A very important point about the S/\sqrt{B} is that it grows with the increase in luminosity \mathcal{L} at the rate of $\sqrt{\mathcal{L}}$. This can be used in extrapolating its values for higher projected luminosities that are going to be achieved in the 13 TeV run-II at the LHC.

3.6 Computational tools

Most of the HEP analyses are performed with ROOT framework which was developed at CERN specifically for this purpose [32]. It is a multi-purpose package that provides tools for big data processing, statistical analysis, visualisation, and storage. It is written in C++ programming language, but also provides integration with other languages such as Python, Ruby, R, etc. ROOT is especially convenient because it provides constructors and methods created specifically for the LHC geometry and the type of analyses it entails. All the computational manipulations and visualisations were performed in ROOT using applications written in C++ and Python.

CHAPTER IV

Determining signal regions

4.1 First view

A common practice in SUSY dilepton analyses is to divide events into same flavour (SF) and different flavour (DF) varieties. SF thus includes events with pairs of only electrons or only muons in their final states, and DF refers to the events that decay into an electron-muon pair. In this analysis this convention will be followed.

The preliminary cuts on the pair of electrons were $\mathbf{p}_{\mathrm{T},e_1} > 25 \text{ GeV}$ and $\mathbf{p}_{\mathrm{T},e_2} > 20 \text{ GeV}$, where e_1 refers to the leading lepton with the largest momentum and e_2 to the second one. For a muon pair the following requirements were imposed: leading muon $\mathbf{p}_{\mathrm{T},\mu_1} > 25 \text{ GeV}$, second muon $\mathbf{p}_{\mathrm{T},\mu_2} > 10 \text{ GeV}$, and the invariant mass $m_{\mu\mu} > 20 \text{ GeV}$. These cuts were motivated by the trigger efficiency for offline lepton candidates' identification (see Fig. A.1 and A.2 in the appendix A).

First, histograms showing the entirety of the 2015 data, MC background and signal simulations were plotted. Fig. 4.1a shows the distribution of the $m_{\ell\ell}$ in the SF channel. The largest background contributions come from the $Z+\text{jets}$, diboson, and $t\bar{t}$ processes. The pronounced peak in the SF dilepton invariant mass distribution is in the 80-100 GeV bin due to the contribution from the $Z+\text{jets}$ component. This background can be suppressed by introducing Z veto which cuts out all events within 10 GeV from the mass of the Z boson (91.2 GeV). However, after this cut, the distribution will still retain events from the off mass-shell decays of the Z boson.

The histogram for DF channel (Fig. 4.1b) shows that there is a much smaller contribution from $Z+\text{jets}$ component in this channel compared to the SF one. Thus Z veto here can be avoided. The diboson and $t\bar{t}$ processes, however, prevail in this channel as well.

The dotted lines are the shapes of signal distributions and they are in accordance with the mass of the chargino pair. The blue line represents 200-150 mass splitting,

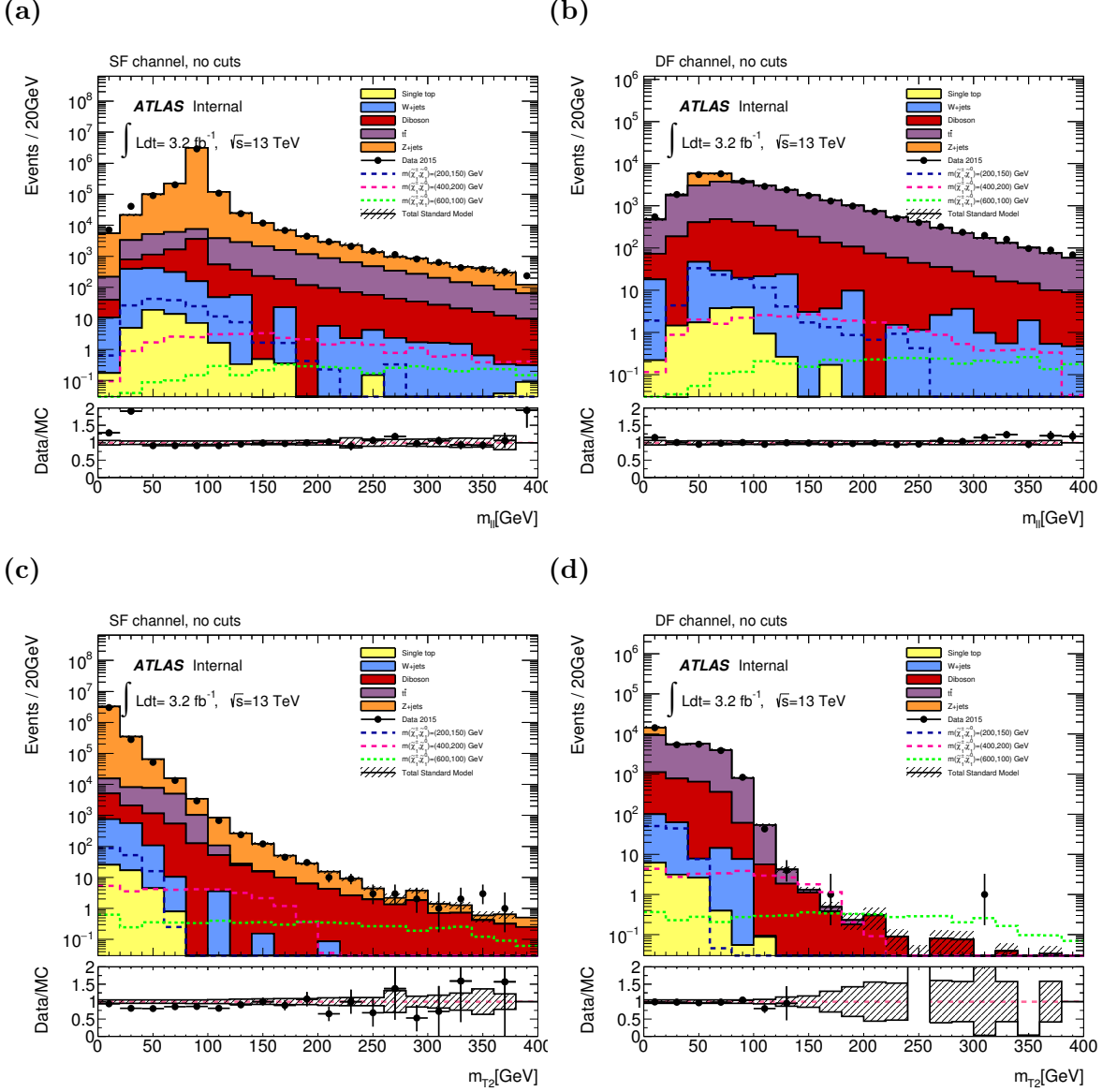


Figure 4.1: Distribution of $m_{\ell\ell}$ and m_{T2} variables for SF and DF channels for all events.

so its events are concentrated in the lower mass regions. The pink and green lines represent 400-200 and 600-100 signals respectively, and also are distributed according to this logic. Overall, there is a good agreement between MC background simulations and the 2015 data.

The total error of the background distribution, shown as hashed lines in the histograms, is calculated using simple poissonian statistics. Full error is a composite estimate that includes all sources of error and their interdependence, it entails a complex analysis that is beyond the scope of this thesis.

4.2 Applying cuts

4.2.1 Veto on all jets.

As was mentioned in the previous section the the following veto was imposed on all the signal regions in SF channel:

$$|m_{\ell\ell} - m_Z| > 10 \text{ GeV} \text{ (with } m_Z = 91.2 \text{ GeV)}$$

This Z veto is common for all further analyses in the SF channel, however it is not used at all for the DF channel. The next step was to veto all the jets to reduce $t\bar{t}$ contribution. The result of this combination of vetoes can be seen in Fig. 4.2. As expected the m_{T2} distribution is dependent on the mass splitting and is better for the 400-200 and 600-100 signals. At this point it is possible to calculate sensitivity values by placing cuts on m_{T2} and the results can be seen in Tab. 4.1. No events from the 200-150 signal model passed the cuts, and therefore it is omitted from the table. The best result for the SF channel was the projected significance of 3.62 at 19.2 fb^{-1} with $m_{T2} > 100 \text{ GeV}$ cut. The same cut for DF channel lead to the significance of 5.15 at $\int \mathcal{L} dt = 19.2 \text{ fb}^{-1}$. Significances for the 600-100 signal were not high in both channels, but were better for DF distributions, although not overwhelmingly so.

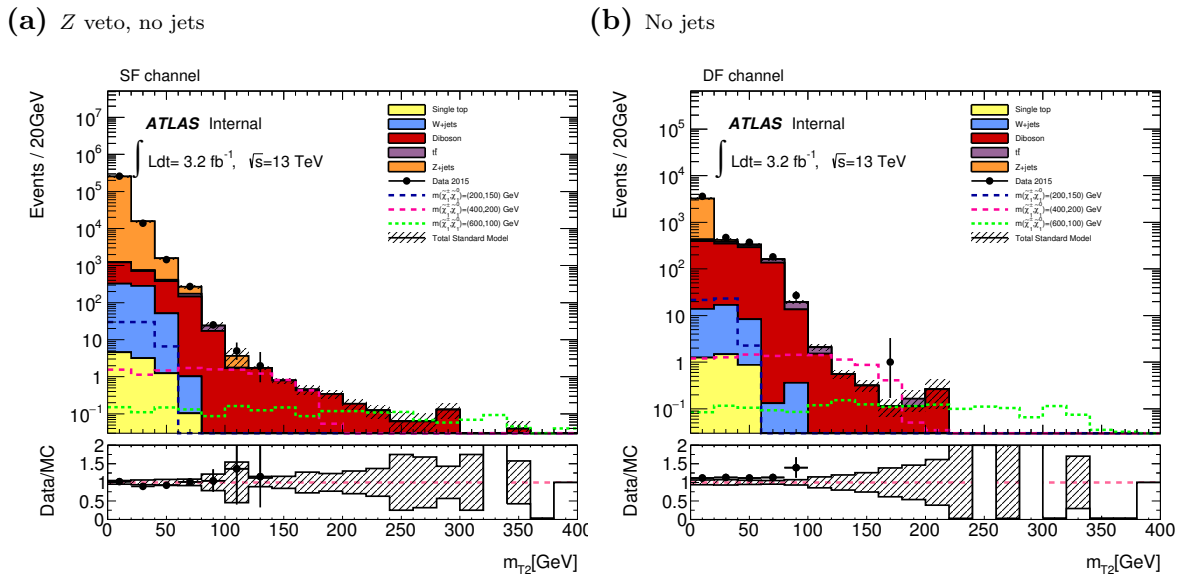


Figure 4.2: The m_{T2} distributions for SF and DF channels, with Z veto (only for SF events) and no jets.

Signal models	400-200	600-100	400-200	600-100	400-200	600-100
$\int \mathcal{L} dt$	3.2 fb ⁻¹		9.6 fb ⁻¹		19.2 fb ⁻¹	
m_{T2} cut [GeV]	SF channel					
> 80	1.01	0.26	1.74	0.45	2.46	0.64
> 100	1.47	0.50	2.56	0.86	3.62	1.22
> 120	1.27	0.61	2.19	1.06	3.09	1.5
	DF channel					
> 80	1.12	0.31	1.95	0.54	2.76	0.76
> 100	2.10	0.75	3.64	1.30	5.15	1.83
> 120	2.10	1.07	3.65	1.86	5.16	2.63

Table 4.1: Significance values (S/\sqrt{B}) for the SF and DF channel signal models with various cuts on m_{T2} at increasing integrated luminosities. Cuts include Z veto (only for SF) and no jets are allowed.

4.2.2 Veto on b -tagged jets.

Instead of vetoing all jets, a different cut vetoing only b -tagged jets was made and the resulting histograms can be seen in Fig. 4.3. The b -jet veto is evidently less drastic and leads to both more background and signal events in the final distribution. In order to see whether this cut makes difference compared to the no-jets cut, the significances have to be calculated. The resulting values can be seen in Table 4.2. Again, no events from the 200-150 signal model passed the cuts and this model was omitted.

The b -jet veto leads to a decrease in significance for SF channel compared to the same cuts with no jets allowed. However, for DF channel significance values are higher. At $\int \mathcal{L} dt = 19$ fb⁻¹ and $m_{T2} > 120$ GeV, the 400-200 signal gives the significance of 6.77, and the 600-100 model has significance of 4.85 for $m_{T2} > 140$ GeV. The difference in response of the SF and DF channels to the b -jet veto is due to the effect of the $Z+jets$ background. It is more prevalent in the SF channel and therefore suppressed better by not allowing jets.

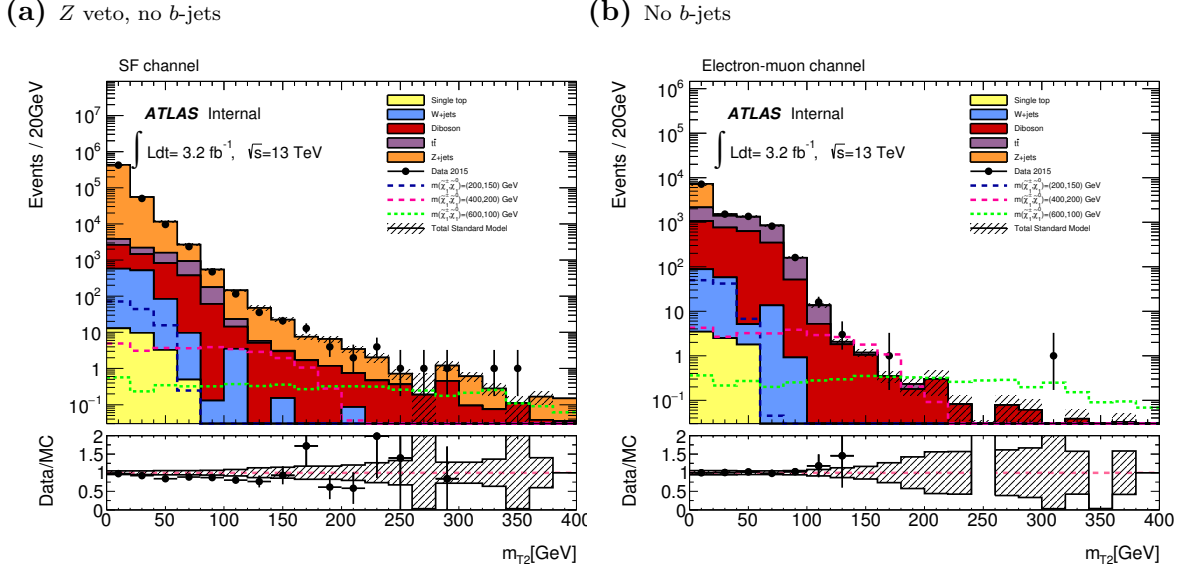


Figure 4.3: The m_{T2} distributions for the SF and DF channels, with Z veto and no b -jets.

Signal models	400-200	600-100	400-200	600-100	400-200	600-100
$\int \mathcal{L} dt$	3.2 fb^{-1}		9.6 fb^{-1}		19.2 fb^{-1}	
m_{T2} cut [GeV]	SF channel					
> 80	0.48	0.14	0.84	0.25	1.19	0.35
> 100	0.63	0.24	1.09	0.41	1.54	0.59
> 120	0.65	0.34	1.12	0.60	1.58	0.84
	DF channel					
> 80	0.94	0.29	1.64	0.50	1.49	0.45
> 100	2.06	0.85	3.57	1.47	5.05	2.08
> 120	2.76	1.59	4.79	2.75	6.77	3.88
> 140	2.07	1.98	3.59	3.43	5.08	4.85

Table 4.2: Significance values for m_{T2} distributions in the SF and DF channels with cuts on m_{T2} at increasing integrated luminosities. With Z veto (SF only) and no b -jets.

4.2.3 Cuts in the same-flavour channel

Further analysis in the SF channel included the already mentioned Z veto and the “no jets” requirement. Different cuts were tried, including limiting jet multiplicity, imposing cuts on $\mathbf{p}_T^{\text{jet}}$, limiting \mathbf{p}_T of the leading jet, etc. Ultimately, most probably due to the high amount of pileup, they were not very efficient. One cut that delivered the best significance values at $\int \mathcal{L} dt = 19.2 \text{ fb}^{-1}$ was requiring $E_T^{\text{miss,rel}} > 80 \text{ GeV}$ and $m_{T2} > 100 \text{ GeV}$ (see Fig. 4.4). This yielded a significance of 4.05 for the 400-200 signal. Requiring $m_{T2} > 120 \text{ GeV}$ gave a significance of 1.50 for the 600-100 signal, the same result as obtained by imposing the $m_{T2} > 120$ cut without the $E_T^{\text{miss,rel}}$ cut (see Tab. 4.1). Tab. 4.3 shows the significance values for these cuts.

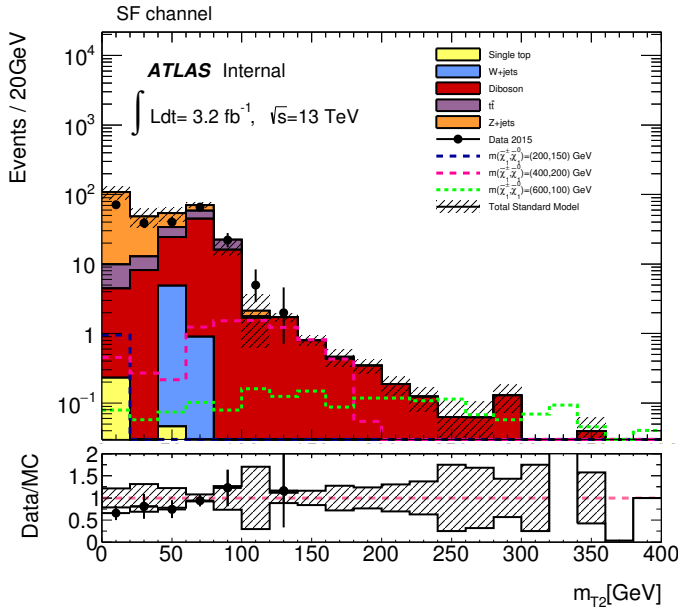


Figure 4.4: The m_{T2} distribution for the SF channel, with Z veto,no jets and $E_T^{\text{miss,rel}} > 80 \text{ GeV}$.

Signal models	400-200	600-100	400-200	600-100	400-200	600-100
$\int \mathcal{L} dt$	3.2 fb^{-1}		9.6 fb^{-1}		19.2 fb^{-1}	
m_{T2} cut [GeV]	SF channel					
> 100	1.65	0.56	2.87	0.97	4.05	1.37
> 120	1.27	0.61	2.19	1.06	3.10	1.50

Table 4.3: Significance values for the SF channel with cut on m_{T2} at increasing integrated luminosities. With Z veto, no jets, and $E_T^{\text{miss,rel}} > 80 \text{ GeV}$.

Overall, significance in the SF channel was low for the two signals that passed the cuts. However, higher luminosities are likely to lead to better sensitivity values for both the 400-200 and 600-100 signal models. There are no significance values for the 200-150 model, although this model has the highest cross-section value. It is in the region which is overwhelmed with background and its suppression is very challenging. One way to deal with this will be discussed in the subsection 4.2.5.

4.2.4 Cuts in the different-flavour channel

The electron-muon signal models overall provide better significance results, and good significance has already been obtained in the simple “no b -jets” plus m_{T2} cut (see Tab. 4.2). However, further investigation was made to see if there is any improvement over those results. For this channel the Z veto does not apply and only b -jets are vetoed.

Higher values for sensitivity for the 400-200 and 600-100 signals were obtained with the following cuts - a) $E_T^{\text{miss,rel}} > 40 \text{ GeV}$ and $m_{T2} > 120 \text{ GeV}$ and b) $E_T^{\text{miss,rel}} > 80 \text{ GeV}$ and $m_{T2} > 120 \text{ GeV}$. The resulting histograms are in Fig. 4.5 and the sensitivities can be seen in the accompanying Table 4.4.

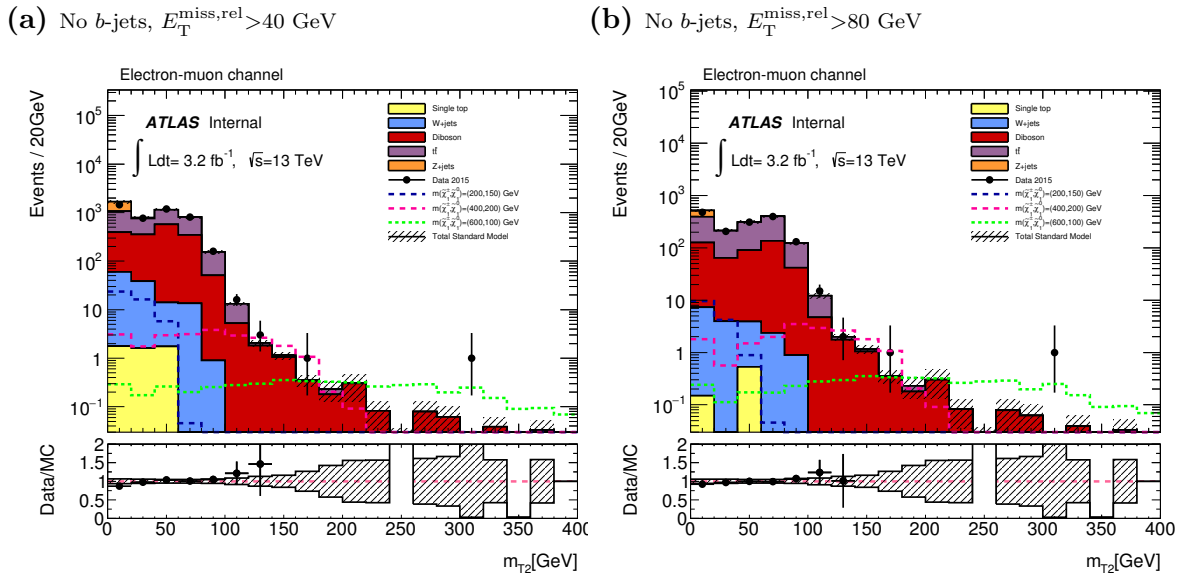


Figure 4.5: The m_{T2} distributions for the DF channel with b -jet veto and different cuts on $E_T^{\text{miss,rel}}$.

Signal models	400-200	600-100	400-200	600-100	400-200	600-100
$\int \mathcal{L} dt$		3.2 fb ⁻¹		9.6 fb ⁻¹		19.2 fb ⁻¹
Cuts	DF channel					
$E_T^{\text{miss,rel}} > 40 \text{ GeV}, m_{T2} > 120 \text{ GeV}$	2.78	1.59	4.81	2.76	6.80	3.90
$E_T^{\text{miss,rel}} > 80 \text{ GeV}, m_{T2} > 120 \text{ GeV}$	2.80	1.61	4.85	2.78	6.86	3.93

Table 4.4: DF channel significances with cuts on m_{T2} and $E_T^{\text{miss,rel}}$ at increasing integrated luminosities. b -jets are vetoed.

The DF channel provides better sensitivity than the SF channel with relatively few cuts. So if the evidence of SUSY lies in this channel it should be relatively easy to confirm. However, this also requires higher luminosity. The 200-150 model does not produce any significance in this channel as well, again due to being in a background-dominated region. The next subsection offers one way this issue can be addressed.

4.2.5 Further investigation of the 200-150 signal

So far, the 200-150 signal proved to be hard to discern from the background. However, there is a method that can potentially yield some sensitivity for this model. It is based on the assumption that the chargino pair creation recoils against a single leading jet which gives additional momentum to the neutralinos in the final state [20]. Thus the angle $\Delta\phi(E_T^{\text{miss}}, \text{jet})$ between E_T^{miss} and the leading jet can be exploited as a discriminating variable. The histograms in Figure 4.6 show this relation for the DF channel.

The 200-150 signal is concentrated at large values for $\Delta\phi(E_T^{\text{miss}}, \text{jet})$ and thereby in agreement with the recoil assumption. However, in these regions the significance values are not high, as can be seen in the Table 4.5.

The best significance value for this search method was 1.47 at 19.2 fb⁻¹ for the $E_T^{\text{miss}} > 80 \text{ GeV}, \Delta\phi(E_T^{\text{miss}}, \text{jet}) > 2.7$ combined cut. It is still quite small and does not satisfy statistical criteria for good sensitivity. However, there is a clear dependence of a smaller mass signal on the recoil angle with the leading jet. This can be a starting point for other analyses that can take into account other variables as well.

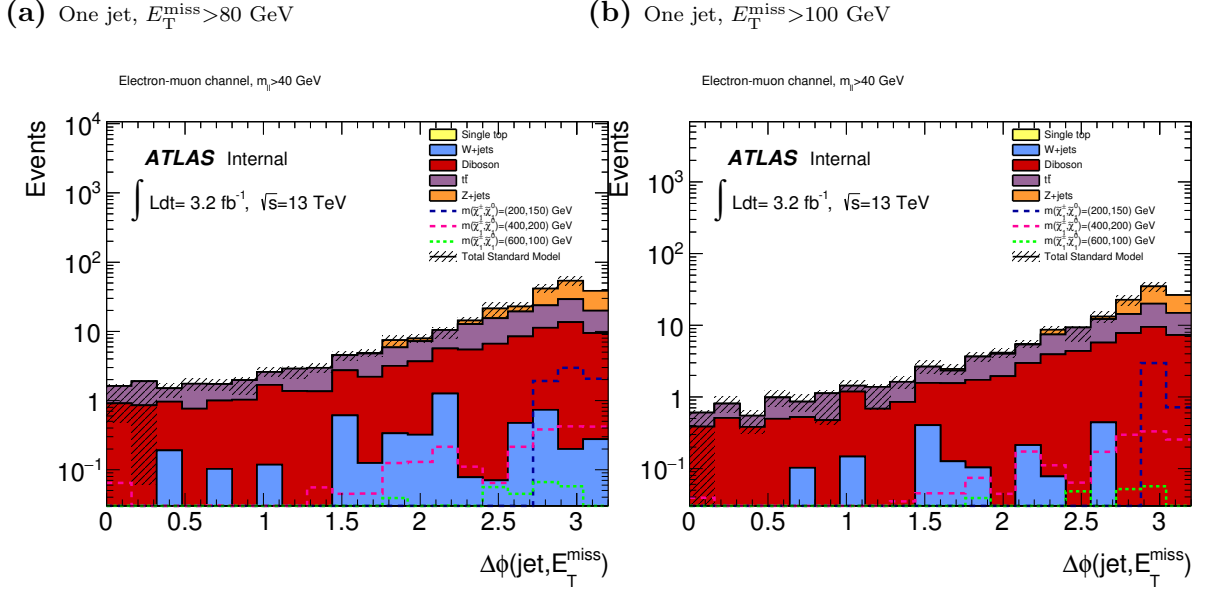


Figure 4.6: The $\Delta\phi(E_T^{\text{miss}}, \text{jet})$ distributions for the DF channel with single jet, $m_{\ell\ell} > 40$ GeV and cuts on E_T^{miss} .

Signal	200-150		
$\int \mathcal{L} dt$	3.2 fb^{-1}	9.6 fb^{-1}	19.2 fb^{-1}
$E_T^{\text{miss}} > 80 \text{ GeV}, \Delta\phi(E_T^{\text{miss}}, \text{jet}) > 2.7$	0.60	1.04	1.47
$E_T^{\text{miss}} > 100 \text{ GeV}, \Delta\phi(E_T^{\text{miss}}, \text{jet}) > 2.9$	0.40	0.70	0.99

Table 4.5: Significances for the $\Delta\phi(E_T^{\text{miss}}, \text{jet})$ distributions for the DF channel with single jet.

CHAPTER V

Conclusion

The search for regions sensitive for specific electroweak SUSY production scenarios was performed in this thesis. The analysis was performed using the 3.2 fb^{-1} of proton-proton collision data gathered at $\sqrt{s} = 13 \text{ TeV}$ in the run-II of the LHC with the ATLAS detector. Various cut strategies were investigated and sensitivities of particular regions to electroweak SUSY production scenarios were analysed.

The previous chapter showed some combinations of cuts that can be used in searches for electroweak SUSY production. For the SF channel the Z veto and no-jets requirement were the starting point and further investigation included cuts on $E_T^{\text{miss,rel}}$ and m_{T2} . For the DF events a veto was placed on b -tagged jets and it was followed by various cuts on $E_T^{\text{miss,rel}}$ and m_{T2} .

The 400-200 GeV mass splitting model provided best values for significance across all combination of cuts. The biggest value was 6.86 for the DF m_{T2} distribution with $E_T^{\text{miss,rel}} > 80 \text{ GeV}$ and $m_{T2} > 120 \text{ GeV}$ at 19.2 fb^{-1} of projected integrated luminosity. The sensitivity for the 600-100 model was lower. The best achieved significance value was 4.85 for the the DF m_{T2} distribution with $m_{T2} > 140 \text{ GeV}$ at 19.2 fb^{-1} of projected integrated luminosity. Finding a sensitive region for the 200-150 signal model proved challenging and no appreciably high significance value was obtained.

These results are in accordance with the theoretical assumptions. Smaller mass charginos have a higher cross section, but their signal resides in regions which are very heavily background-dominated. Higher mass charginos have a larger presence in the tails of distributions but possess much smaller cross sections and therefore produce fewer events. Thus, the fact that the intermediate signal showed the best sensitivity is not surprising. It strikes a balance between having a large enough cross section and extending into regions which are not that heavily populated with background events.

The significance values at the current gathered data luminosity of 3.2 fb^{-1} show that there is little sensitivity to the SUSY processes discussed in this thesis. However,

at the projected luminosity value of 19.2 fb^{-1} there is a marked improvement in significance, especially in the DF channel. With the LHC continuing its run at 13 TeV more data will become available and this will undoubtedly improve the sensitivity to the SUSY scenarios.

CHAPTER VI

Critical reflection

The process of doing research for this thesis has certainly been beneficial for me in several regards. I became familiar with techniques used for HEP analysis. Several crucial skills were obtained and they are going to be immensely helpful in my future career. These include

1. Learning to work on Linux OS, which included interacting via `bash` to connect to CERN servers and run scripts.
2. Learning the basics of the C++ programming language.
3. Learning to effectively manage produced data.

Although the project was concluded on time, I feel that my time could have been spent more productively, especially in the first half of the thesis period. A lot of time then was spent on revising things, and , in hidnsight, that could have taken much less time. Among personal shortcomings I would like to point out that communication from my side could have been much better. Many issues in the beginning and further on could have been avoided if I articulated my problems and questions earlier. This way I could have achieved more with this thesis. My time management skills need to be improved as well. Procrastination is very punishing on the quality of work and the resulting text.

Overall, doing this research was very enjoyable. It also was challenging and prompted me to acquire knowledge and skills I will certainly use in the future.

I would like to thank Dr. Sara Williams for providing me with this opportunity and being a wonderful thesis supervisor.

APPENDICES

APPENDIX A

Trigger Efficiencies

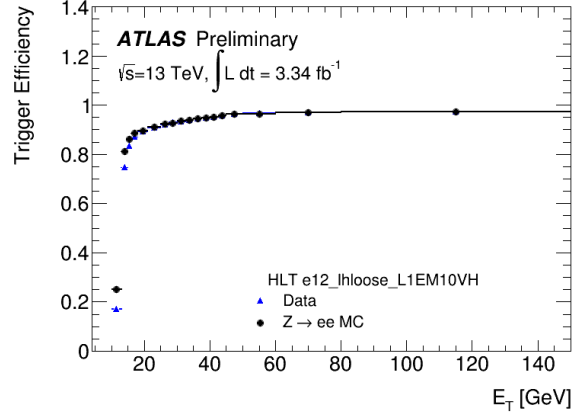


Figure A.1: Electron trigger efficiency as a function of the offline electron candidates E_T [33].

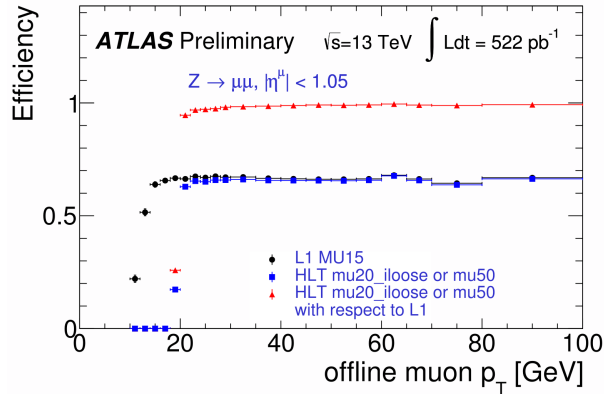


Figure A.2: Muon trigger efficiency as a function of p_T of offline muon candidates [34].

Bibliography

- [1] G. Aad *et al.*, “Observation of a new particle in the search for the Standard Model Higgs boson with the ATLAS detector at the LHC,” *Phys. Lett.*, vol. B716, pp. 1–29, 2012.
- [2] S. Chatrchyan, V. Khachatryan, A. M. Sirunyan, A. Tumasyan, W. Adam, E. Aguilo, T. Bergauer, M. Dragicevic, J. Erö, C. Fabjan, *et al.*, “Observation of a new boson at a mass of 125 gev with the cms experiment at the lhc,” *Physics Letters B*, vol. 716, no. 1, pp. 30–61, 2012.
- [3] B. R. Martin, *Nuclear and particle physics: An introduction*. John Wiley & Sons, 2006.
- [4] S. L. Glashow, “Partial Symmetries of Weak Interactions,” *Nucl. Phys.*, vol. 22, pp. 579–588, 1961.
- [5] S. Weinberg, “A model of leptons,” *Physical review letters*, vol. 19, no. 21, p. 1264, 1967.
- [6] A. Salam and N. Svartholm, “Elementary particle theory,” *Almqvist and Wiksell, Stockholm*, p. 367, 1968.
- [7] F. Englert and R. Brout, “Broken symmetry and the mass of gauge vector mesons,” *Physical Review Letters*, vol. 13, no. 9, p. 321, 1964.
- [8] P. W. Higgs, “Broken symmetries and the masses of gauge bosons,” *Physical Review Letters*, vol. 13, no. 16, p. 508, 1964.
- [9] E. Gildener, “Gauge-symmetry hierarchies,” *Phys. Rev. D*, vol. 14, pp. 1667–1672, Sep 1976.
- [10] P. A. Ade, N. Aghanim, M. Alves, C. Armitage-Caplan, M. Arnaud, M. Ashdown, F. Atrio-Barandela, J. Aumont, H. Aussel, C. Baccigalupi, *et al.*, “Planck 2013 results. I. overview of products and scientific results,” *Astronomy & Astrophysics*, vol. 571, p. A1, 2014.
- [11] CMS , “Are there more particles left to find? supersymmetry: uniting the forces,” 2011. [Online; accessed May 18, 2016].

- [12] J. D. Lykken, “Introduction to supersymmetry,” in *Fields, strings and duality. Proceedings, Summer School, Theoretical Advanced Study Institute in Elementary Particle Physics, TASI'96, Boulder, USA, June 2-28, 1996*, pp. 85–153, 1996.
- [13] G. Aad, E. Abat, J. Abdallah, A. Abdelalim, A. Abdesselam, O. Abdinov, B. Abi, M. Abolins, H. Abramowicz, E. Acerbi, *et al.*, “The atlas experiment at the cern large hadron collider,” *Journal of Instrumentation*, vol. 3, no. 8, 2008.
- [14] G. Aad, B. Abbott, J. Abdallah, A. Abdelalim, A. Abdesselam, O. Abdinov, B. Abi, M. Abolins, H. Abramowicz, H. Abreu, *et al.*, “The atlas inner detector commissioning and calibration,” *The European Physical Journal C*, vol. 70, no. 3, pp. 787–821, 2010.
- [15] Pequenao, Joao, “Event cross section in a computer generated image of the atlas detector.,” 2008. [Online; accessed May 18, 2016].
- [16] G. Aad, B. Abbott, J. Abdallah, A. Abdelalim, A. Abdesselam, O. Abdinov, B. Abi, M. Abolins, H. Abramowicz, H. Abreu, *et al.*, “Performance of the atlas trigger system in 2010,” *The European Physical Journal C*, vol. 72, no. 1, pp. 1–61, 2012.
- [17] G. Barr, R. Devenish, R. Walczak, and T. Weidberg, *Particle Physics in the LHC Era*. Oxford University Press, 2015.
- [18] C. Borschensky, M. Krämer, A. Kulesza, M. Mangano, S. Padhi, T. Plehn, and X. Portell, “Squark and gluino production cross sections in pp collisions at $\sqrt{s}=13, 14, 33$ and 100 tev,” *The European Physical Journal C*, vol. 74, no. 12, pp. 1–12, 2014.
- [19] G. Aad, B. Abbott, J. Abdallah, O. Abdinov, R. Aben, M. Abolins, O. AbouZeid, H. Abramowicz, H. Abreu, R. Abreu, *et al.*, “Summary of the searches for squarks and gluinos using $\sqrt{s} = 8$ tev pp collisions with the atlas experiment at the lhc,” *Journal of High Energy Physics*, vol. 2015, no. 10, pp. 1–100, 2015.
- [20] G. Aad *et al.*, “Search for the electroweak production of supersymmetric particles in $\sqrt{s}=8$ TeV pp collisions with the ATLAS detector,” *Phys. Rev.*, vol. D93, no. 5, p. 052002, 2016.
- [21] ATLAS collaboration, “Mass reach of atlas searches for supersymmetry,” 2016.
- [22] G. Aad, B. Abbott, J. Abdallah, O. Abdinov, R. Aben, M. Abolins, O. AbouZeid, H. Abramowicz, H. Abreu, R. Abreu, *et al.*, “Search for the electroweak production of supersymmetric particles in $s=8$ tev p p collisions with the atlas detector,” *Physical review D*, vol. 93, no. 5, p. 052002, 2016.
- [23] B. Fuks, M. Klasen, D. R. Lamprea, and M. Rothering, “Gaugino production in proton-proton collisions at a center-of-mass energy of 8 TeV,” *JHEP*, vol. 10, p. 081, 2012.

- [24] B. Fuks, M. Klasen, D. R. Lamprea, and M. Rothering, “Precision predictions for electroweak superpartner production at hadron colliders with RESUMMINO,” *Eur. Phys. J. C*, vol. 73, p. 2480, 2013.
- [25] ATLAS Collaboration, “Nlo-nll wino-like chargino-chargino (c1c1) cross sections.” <https://twiki.cern.ch/twiki/bin/view/LHCPhysics/SUSYCrossSections13TeVx1x1wino>, 2016.
- [26] W. Wagner, “Top-Antitop-Quark Production and Decay Properties at the Tevatron,” *Mod. Phys. Lett.*, vol. A25, pp. 1297–1314, 2010.
- [27] Z. Marshall, “Simulation of Pile-up in the ATLAS Experiment,” *J. Phys. Conf. Ser.*, vol. 513, p. 022024, 2014.
- [28] G. Aad *et al.*, “Search for supersymmetry at $\sqrt{s} = 13$ TeV in final states with jets and two same-sign leptons or three leptons with the ATLAS detector,” *Eur. Phys. J.*, vol. C76, no. 5, p. 259, 2016.
- [29] G. Aad *et al.*, “Performance of b -Jet Identification in the ATLAS Experiment,” *JINST*, vol. 11, no. 04, p. P04008, 2016.
- [30] C. G. Lester and D. J. Summers, “Measuring masses of semiinvisibly decaying particles pair produced at hadron colliders,” *Phys. Lett.*, vol. B463, pp. 99–103, 1999.
- [31] A. Barr, C. Lester, and P. Stephens, “ $m(T2)$: The Truth behind the glamour,” *J. Phys.*, vol. G29, pp. 2343–2363, 2003.
- [32] “ROOT Data Analysis Framework.” <https://root.cern.ch/>.
- [33] ATLAS Collaboration, “Electron trigger performance in 2015 ATLAS data (December 6, 2015) .” https://twiki.cern.ch/twiki/bin/view/AtlasPublic/EgammaTriggerPublicResults#Electron_trigger_performance_AN2.
- [34] ATLAS Collaboration, “Muon trigger performances in 2015 25ns data-taking period.” https://twiki.cern.ch/twiki/bin/view/AtlasPublic/MuonTriggerPublicResults#Muon_trigger.Performances_in_2015.